Bond Dissociation Energies and Equilibrium Structures of $Cu^+(MeOH)_x$, $x = 1-6$, in the Gas Phase: Competition between Solvation of the Metal Ion and Hydrogen-Bonding Interactions

Z. Yang, N. S. Rannulu, Y. Chu, and M. T. Rodgers*

Department of Chemistry, Wayne State University, Detroit, Michigan 48202

Received: August 30, 2007; In Final Form: October 22, 2007

The solvation of Cu^+ by methanol (MeOH) was studied via examination of the kinetic energy dependence of the collision-induced dissociation of $Cu^+(MeOH)_x$ complexes, where $x = 1-6$, with Xe in a guided ion beam tandem mass spectrometer. In all cases, the primary and lowest-energy dissociation channel observed is the endothermic loss of a single MeOH molecule. The primary cross section thresholds are interpreted to yield 0 and 298 K bond dissociation energies (BDEs) after accounting for the effects of multiple ion−neutral collisions, kinetic and internal energy distributions of the reactants, and lifetimes for dissociation. Density functional theory calculations at the B3LYP/6-31G* level are performed to obtain model structures, vibrational frequencies, and rotational constants for the $Cu^+(MeOH)_x$ complexes and their dissociation products. The relative stabilities of various conformations and theoretical BDEs are determined from single-point energy calculations at the B3LYP/6-311+G(2d,2p) level of theory using B3LYP/6-31G*-optimized geometries. The relative stabilities of the various conformations of the $Cu^+(MeOH)_x$ complexes and the trends in the sequential BDEs are explained in terms of stabilization gained from sd hybridization, hydrogen-bonding interactions, electron donor−acceptor natural bond orbital stabilizing interactions, and destabilization arising from ligand−ligand repulsion.

Introduction

Electrospray ionization (ESI) has become an extremely versatile and increasingly popular ionization technique for mass spectrometry (MS) analyses. It is ideally suited for studies of biochemical systems because it allows for large, nonvolatile molecules to be ionized and analyzed directly from solution. Therefore, ESI can be coupled to separation techniques such as high-performance liquid chromatography and capillary electrophoresis.[1−3] The composition of solutions employed in ESI analyses should be chosen judiciously to ensure that a stable spray can be generated while providing adequate ion intensities for the analyte(s) of interest. An important characteristic of suitable ESI solvents is that their surface tensions lie within the range that facilitates the generation of a stable spray. It is generally easy to create and maintain a stable spray in the positive ion mode with conductive solutions comprised of greater than 50% of a moderately polar organic solvent (e.g., methanol), with the remainder of the solvent being aqueous.[4−6] Therefore, studies of the interactions of analyte molecules and solutes present in the ESI solution (e.g., metal ions derived from dissolved salts) with solvent molecules are of interest. Likewise, knowledge of the thermochemistry relevant to these interactions may be useful for the rational selection of solutions that can be productively employed for ESI analyses. Such reliable thermochemical data may also provide a means by which a better understanding of the ionization processes that occur in ESI might be elucidated.

A wide variety of transition-metal ions play active roles in biological processes, being components of proteins, nucleic acids, vitamins, and drugs.[7,8] Copper is essential for many processes in bioorganisms and plays an important role in many enzymatic processes.[9] For example, copper is involved in the action of cytochrome-*c* oxidase, lactase,[10] Cu, Zn superoxidase dismutase, ceruloplasmin, diammineoxidase, azurin,[11] and indophenol oxidase or tyrosinase.[12] In addition, Cu^+/Cu^{2+} redox reaction electron-transfer systems, in which the copper cation is usually coordinated to the side chains of cysteine and histidine residues, are the active centers of blue copper proteins and have been extensively studied by various theoretical and experimental methods.[13−16] Therefore, the study of Cu^+−ligand interactions may provide insight into the interactions that control structure and function in large biological systems in which copper ions play a role. Such biologically relevant Cu^+−ligand interactions have been extensively studied for a variety of simple biologically relevant ligands including the nucleic acid bases[17−20] and amino acids.[21−29] Copper ions in water or ammonia solutions have also been investigated by static[30,31] and dynamic[32,33] approaches and ab initio calculations.[34−36] Gas-phase studies of the interactions of Cu^+ and Cu^{2+} with a variety of solvents including water,[37−41] ammonia,[37,42−44] acetonitrile,[45] acetone,[46] dimethylether,[47] imidazole,[48] and pyridine[49] molecules have also been reported. One advantage of gas-phase studies is that they allow the direct determination of the strength of the intrinsic interactions between the copper ion and the ligand molecule(s) in the absence of solvents effects. However, the binding in solution can differ markedly from that observed in the gas phase as a result of the influence of solvent on these interactions. In general, the solvent significantly weakens electrostatic forces (and hydrogen-bonding interactions, when present) between ions and ligands by shielding and competing for their interactions. The relative behavior in solution often parallels that of the gas phase, but in some cases, a marked change in the relative binding affinities is observed. By measuring the strength of noncovalent interactions both in solution and in the gas phase, the influence of the solvent on such interactions can, in principle, be elucidated.

10.1021/jp076964v CCC: $40.75
Published on Web 01/03/2008

In recent work, we have developed methods to allow the application of quantitative threshold collision-induced dissociation (CID) methods to obtain accurate thermodynamic information on increasingly large systems, such as the solvation of metal ions by a variety of solvents.[45,46,48−52] In the current study, we examine the solvation of Cu^+ by methanol (MeOH) via characterization of the CID behavior, structures, and energetics of binding in $Cu^+(MeOH)_x$ complexes, where $x = 1-6$. The kinetic-energy-dependent cross sections for the CID processes are analyzed using methods developed previously.[53] The analysis explicitly includes the effects of the internal and translational energy distributions of the reactants, multiple ion−neutral collisions, and the lifetime for dissociation. We derive $(MeOH)_{x-1}Cu^+-MeOH$ bond dissociation energies (BDEs) for all of the complexes, $x = 1-6$, and compare these results to density functional theory calculations (B3LYP) performed here. The nature of the bonding interactions and the trends in the sequential BDEs of Cu^+ to MeOH calculated and measured here are examined in detail to elucidate the factors that contribute to the binding in these systems. The trends in the $Cu^+(MeOH)_x$ BDEs are also compared to those found for a variety of other solvents or ligands binding to Cu^+ previously examined, including water,[39] ammonia,[44] acetonitrile,[45] acetone,[46] dimethylether,[47] imidazole,[48] and pyridine.[49]

Experimental Section

Experimental Protocol. The guided ion beam tandem mass spectrometer in which these experiments were performed has been described in detail elsewhere.[54] The $Cu^+(MeOH)_x$ complexes are generated by condensation of Cu^+, generated via dc discharge, with one to six neutral MeOH molecules. The $Cu^+(MeOH)_x$ complexes are collisionally stabilized and thermalized by $>10^5$ collisions with the He and Ar bath gases, such that their internal energies are believed to be well described by a Maxwell−Boltzmann distribution at room temperature. The $Cu^+(MeOH)_x$ complexes are effusively sampled from the source, focused, accelerated, and focused into a magnetic sector momentum analyzer for reactant ion mass selection. The mass-selected ions are decelerated to a desired kinetic energy and injected into an octopole ion beam guide, which traps the ions in the radial direction. The octopole ion beam guide acts as an efficient radial ion trap such that loss of reactant and product ions as they drift through the octopole is almost entirely eliminated.[55,56] The octopole passes through a static gas cell containing Xe at a sufficiently low pressure (∼0.05−0.20 mTorr) that multiple ion−neutral collisions are improbable. Unreacted beam and product ions drift to the end of the octopole and are focused into a quadrupole mass filter for mass analysis and subsequently detected with a secondary electron scintillation detector using standard pulse counting techniques.

Data Handling. Ion intensities are converted to absolute cross sections using a Beer's law analysis.[57] Uncertainties in the absolute cross sections are estimated to be ±20%, which are largely the result of errors in the pressure measurement and uncertainties in the length of the interaction region. Relative uncertainties are approximately ±5%.

Ion kinetic energies in the laboratory frame, E_{lab}, are converted into energies in the center-of-mass frame, E_{cm}, using the formula $E_{cm} = E_{lab}(m/(m + M))$, where M and m are the masses of the ionic and neutral reactants, respectively. All energies reported below are in the center-of-mass frame unless otherwise noted. The absolute zero and distribution of the ion kinetic energies are determined using the octopole ion guide as a retarding potential analyzer, as previously described.[57] The distribution of ion kinetic energies is nearly Gaussian, with a fwhm in the range from 0.3 to 0.4 eV (lab) for these experiments. The absolute uncertainty in the energy scale is ±0.05 eV.

Because multiple ion−neutral collisions can influence the shape of CID cross sections and the threshold regions are most sensitive to these effects, each CID cross section was measured twice at three nominal Xe pressures (0.05, 0.10, and 0.20 mTorr). Data free from pressure effects are obtained by extrapolating to zero reactant pressure, as described previously.[39] Thus, cross sections subjected to thermochemical analysis are due to single bimolecular encounters.

Theoretical Calculations. Density functional theory calculations were performed using Gaussian 98[58] to obtain model structures, vibrational frequencies, rotational constants, and energetics for neutral MeOH and the $Cu^+(MeOH)_x$ complexes, where $x = 1-6$. Geometry optimizations and frequency analyses of the optimized structures were performed at the B3LYP/6-31G* level.[59,60] When used to model the data or to calculate thermal energy corrections, the B3LYP/6-31G* vibrational frequencies are prescaled by a factor of 0.9804.[61−63] The prescaled vibrational frequencies for these systems are listed in the Supporting Information in Table 1S. Single-point energy calculations were performed at the B3LYP/6-311+G(2d,2p) level using the B3LYP/6-31G*-optimized geometries. Zero point energy (ZPE) and basis set superposition error (BSSE) corrections are included in the calculated BDEs.[64,65]

A wide variety of initial geometries for the $Cu^+(MeOH)_x$ complexes were investigated to ensure that conformational space was adequately probed, competition between solvation of the metal ion and hydrogen-bonding interactions was accurately assessed, and the ground-state conformations of these species were accurately determined. In particular, for each $Cu^+(MeOH)_x$ complex, initial conformations in which the number of MeOH molecules directly bound to Cu^+ was continuously varied from one to x, with the remaining MeOH molecules hydrogen-bound to the central ion core, were examined. All initial structures that involved more than four MeOH molecules directly bound to Cu^+ always converged to structures involving only four MeOH molecules directly bound to Cu^+, with the fifth (and sixth) MeOH molecules occupying sites in the first solvent shell. Although we believe we have determined appropriate ground-state conformations for these complexes, we are aware that we may not have calculated or identified all low-energy conformations available to these species.

Natural Bond Orbital Analyses. Natural bond orbitals (NBOs) are the localized few-center orbitals (typically 1 or 2, but occasionally more) that describe the Lewis-like molecular bonding pattern of electron pairs (or of individual electrons in the open-shell case) in an optimally compact form. A NBO analysis is based on a method for optimally transforming a given wave function into a localized form, corresponding to the one-center ("lone pair") and two-center ("bond") elements of the chemist's Lewis structure picture. Thus, NBOs provide a valence bond-type description of the wave function such that the ab initio computational results can be closely linked to classical Lewis structure concepts. The NBO program[66] in Gaussian 98[58] was used to analyze the many-electron molecular wave functions in terms of localized electron-pair "bonding" units and provide all possible interactions between filled Lewis-type electron−donor NBOs with non-Lewis electron−acceptor NBOs. These types of interactions, termed the "stabilization energy" ($E(2)$), are estimated using second-order perturbation theory. In this study, we performed NBO analyses for all of the ground-state structures and several of the low-lying excited conformations

of the $Cu^+(MeOH)_x$ complexes to examine the nature of the binding in these complexes and to provide insight into the relative stabilities of the various conformations and sequential BDEs of these systems.

Thermochemical Analysis. The threshold regions of the CID reaction cross sections are modeled using eq 1

$$\sigma(E) = \sigma_0 \sum_i g_i(E + E_i - E_0)^n/E \quad (1)$$

where σ_0 is an energy-independent scaling factor, E is the relative kinetic energy of the reactants, E_0 is the threshold for reaction of the ground electronic and rovibrational state, and n is an adjustable parameter that describes the efficiency of kinetic to internal energy transfer.[67] The summation is over the rovibrational states of the reactant ions, i, having energies, E_i, and populations, g_i, where $\sum g_i = 1$.

The Beyer−Swinehart algorithm[68] is used to determine the density of rovibrational states, and the relative populations, g_i, are calculated for a Maxwell−Boltzmann distribution at 298 K, the internal temperature of the reactants. The vibrational frequencies are determined from electronic structure calculations, as discussed in the Theoretical Calculations section. The average vibrational energies at 298 K of neutral MeOH and the ground-state $Cu^+(MeOH)_x$ complexes, where $x = 1-6$, are given in the Supporting Information in Table 1S. We have increased and decreased the vibrational frequencies (prescaled by 0.9804) by 10% to encompass the range of average scaling factors needed to bring the calculated frequencies into agreement with the experimentally determined frequencies.[69] The corresponding change in the average vibrational energy is taken to be an estimate of one standard deviation of the uncertainty in the vibrational energy (Table 1S).

Statistical theories for unimolecular dissociation (Rice−Ramsperger−Kassel−Marcus (RRKM) theory) of the collisionally activated ions are also included in eq 1 to account for the possibility that these ions may not have undergone dissociation prior to arriving at the detector ($\sim 10^{-4}$ s).[51,70] In our analyses, we assume that the transition states (TSs) are loose and product-like because the interaction between Cu^+ and the MeOH molecules is largely electrostatic. The best model for the TS of such electrostatically bound complexes is a loose phase space limit (PSL) model located at the centrifugal barrier for the interaction of the products, $Cu^+(MeOH)_{x-1}$ and MeOH, as described in detail elsewhere.[53] The molecular parameters appropriate for the PSL model TS are therefore the frequencies and rotational constants of the products. Vibrational frequencies and rotational constants appropriate for the energized molecules and the TSs leading to dissociation are given in the Supporting Information in Tables 1S and 2S.

The model represented by eq 1 is expected to be appropriate for translationally driven reactions[71] and has been found to reproduce CID cross sections well. The model is convoluted with the kinetic energy distributions of both the reactant $Cu^+(MeOH)_x$ complex and neutral Xe atom, and a nonlinear least-squares analysis of the data is performed to give optimized values for the parameters σ_0, E_0 and E_0(PSL), and n. The errors associated with the measurement of E_0 and E_0(PSL) are estimated from the range of threshold values determined for the zero-pressure-extrapolated data sets, variations associated with uncertainties in the vibrational frequencies (scaling as discussed above), and the error in the absolute energy scale, 0.05 eV (lab). For analyses that include the RRKM lifetime analysis, the uncertainties in the reported E_0(PSL) values also include the effects of increasing and decreasing the time assumed available for dissociation by a factor of 2.

Equation 1 explicitly includes the internal energy of the ion, E_i. All energy available is treated statistically because the internal energy of the reactants is redistributed throughout the $Cu^+(MeOH)_x$ complex upon collision with Xe. Because the CID processes examined here are simple noncovalent bond fission reactions, the E_0(PSL) values determined by analysis with eq 1 can be equated to 0 K BDEs.[72,73]

Results

Cross Sections for Collision-Induced Dissociation. Experimental cross sections were obtained for the interaction of Cu^+ with one to six MeOH molecules. The sequential loss of intact MeOH molecules and ligand exchange with Xe are the only processes observed for the $Cu^+(MeOH)_x$ complexes, where $x = 1-6$, over the energy range examined, typically 0−10 eV. Figure 1 shows data for all six $Cu^+(MeOH)_x$ complexes. The most favorable process for all complexes is the loss of a single MeOH molecule in the CID reactions 2

$$Cu^+(MeOH)_x + Xe \rightarrow Cu^+(MeOH)_{x-1} + MeOH + Xe \quad (2)$$

The maximum cross section for reactions 2 (as well as the total cross section) increases in magnitude as the size of the $Cu^+(MeOH)_x$ complex increases, from ~6.1 to 19 to 52 to 65 to 70 to 86 Å^2 for $x = 1-6$, respectively. In contrast, the threshold for reaction 2 increases slightly from $x = 1$ to 2, decreases sharply from $x = 2$ to 3, and then decreases slowly with further increases in the size of the complex. This behavior has been observed for other transition-metal ions binding to a variety of different ligands previously examined[34,37−39,42−49] and can be explained in terms of sd hybridization effects, as discussed below.

Dissociation of additional MeOH ligands is observed for the larger $Cu^+(MeOH)_x$ complexes at elevated energies. The shapes of the CID product cross sections confirm that these species are formed sequentially from the larger complexes, that is, the primary product, $Cu^+(MeOH)_{x-1}$, decreases as the secondary product, $Cu^+(MeOH)_{x-2}$ begins to appear. Similar behavior is observed for the higher-order dissociation processes. For the $Cu^+(MeOH)_x$ complexes, where $x = 1-5$, complete dissociation of the reactant $Cu^+(MeOH)_x$ complex to produce bare Cu^+ is observed. As the size of the cluster increases, higher-order dissociation (secondary, tertiary, etc.) accounts for a greater percentage of the total cross section, approximately ~5, 23, 52, 50, and 57% for $x = 2$, 3, 4, 5, and 6, respectively, at the highest energies examined. In general, the cross section magnitudes decrease from the primary to secondary to tertiary to quaternary to quinary dissociation product at all energies examined. However, deviation from this behavior occurs for the $Cu^+(MeOH)_x$ complexes, where $x = 4-6$, where the $Cu^+(MeOH)_2$ and $Cu^+(MeOH)_3$ product cross sections are observed to cross at ~3.0 eV such that the magnitude of the $Cu^+(MeOH)_2$ product is larger than that of the $Cu^+(MeOH)_3$ product at high energies. This may be the result of sd hybridization effects that lead to very strong binding for the first two ligands, as discussed below. Oddly, these two product ions exhibit very similar thresholds, which may indicate the presence of a minor contaminant in the reactant ion beam that forms an ion isobaric with $Cu^+(MeOH)_2$. Because these product ions are not involved in the threshold analysis described below, such a contaminant will not affect the results.

The cross sections for ligand exchange decrease as the size of the $Cu^+(MeOH)_x$ complex increases. For the case of $x = 1$, the cross section for the ligand exchange process is substantial,

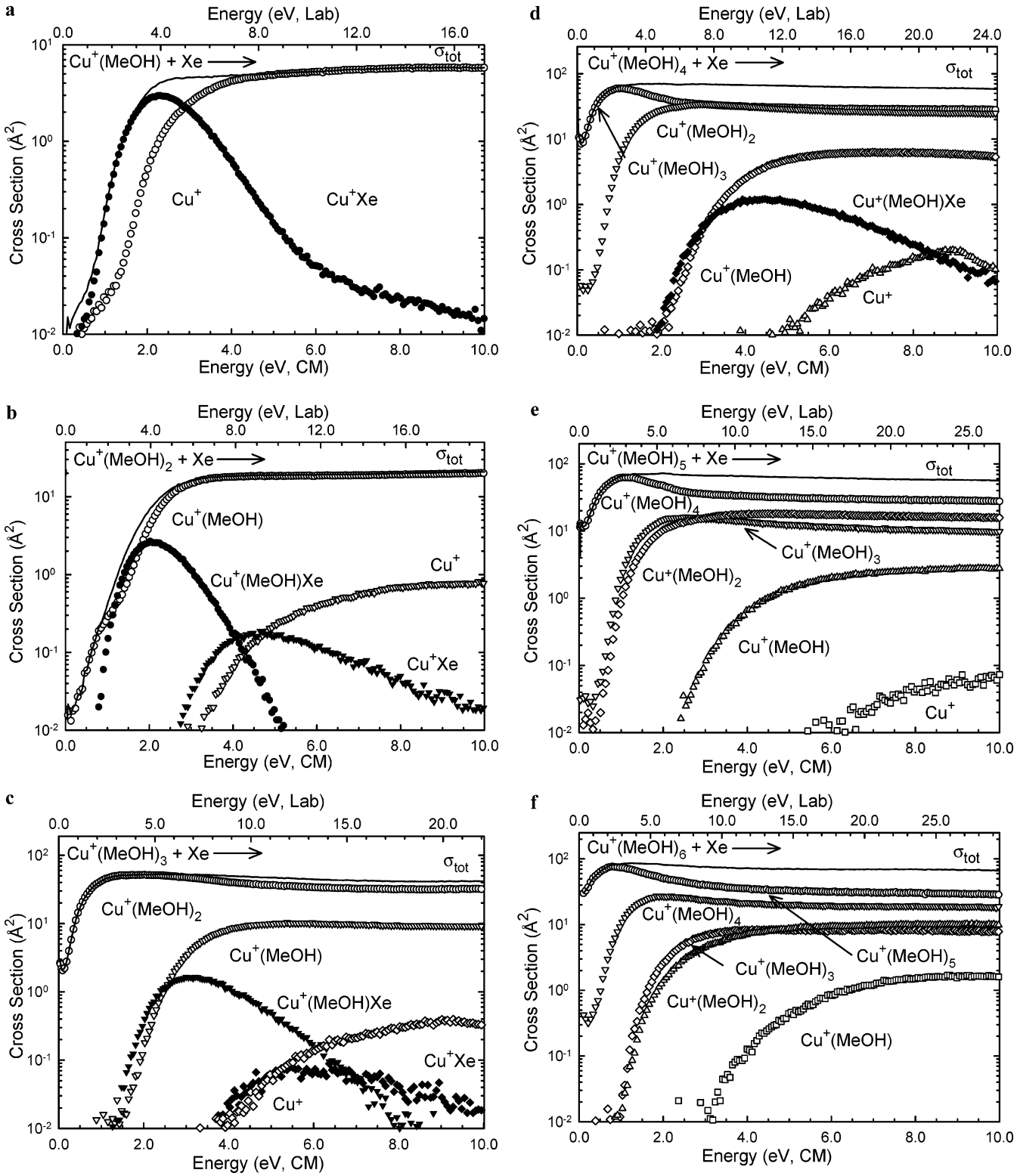

Figure 1. Cross sections for collision-induced dissociation of the $Cu^+(MeOH)_x$, where $x = 1-6$, with Xe as a function of the kinetic energy in the center-of-mass frame (lower x axis) and laboratory frame (upper x axis), parts a through f, respectively. Primary, secondary, tertiary, quaternary, and quinary CID and ligand exchange product cross sections are shown as ○, ▽, ◇, △, and □ and ●, ▼, and ◆, respectively.

having a maximum that is ~60% as large as the CID process. The magnitude of the ligand exchange cross section for the $Cu^+(MeOH)_2$ complex is ~70% as large as that observed for the $Cu^+(MeOH)$ complex, but its contribution to the total cross section has dropped, such that it accounts for ~40% of the total cross section. Similarly, the ligand exchange cross sections continue to decrease with increasing ligation such that for the $Cu^+(MeOH)_3$ and $Cu^+(MeOH)_4$ complexes, the ligand exchange processes account for less than 3 and 2% of the total cross section, respectively. For the $Cu^+(MeOH)_5$ and $Cu^+(MeOH)_6$ complexes, the ligand exchange processes could not be differentiated from background noise.

Threshold Analysis. The threshold regions for CID reactions 2 in six $Cu^+(MeOH)_x$ complexes were analyzed using the model of eq 1. In general, the analysis of the primary CID threshold provides the most reliable thermochemistry because secondary

TABLE 1: Fitting Parameters of Eq 1, Threshold Dissociation Energies at 0 K, and Entropies of Activation at 1000 K[a]

species	σ_0[b]	n[b]	E_0[c] (eV)	E_0(PSL)[b,d] (eV)	kinetic shift[e] (eV)	$\Delta S^\dagger$ (J mol^{-1} K^{-1})
$Cu^+(MeOH)$	4.2 (0.4)	1.5 (0.1)	1.85 (0.03)	1.85 (0.03)	<0.01	29 (2)
$Cu^+(MeOH)_2$	29.6 (2.5)	1.3 (0.1)	2.01 (0.08)	1.94 (0.07)	0.07	45 (5)
$Cu^+(MeOH)_3$	73.6 (2.8)	1.1 (0.1)	0.75 (0.04)	0.74 (0.03)	0.01	42 (3)
	74.1 (3.4)[f]	1.0 (0.1)[f]	0.78 (0.03)[f]	0.75 (0.03)[f]	0.03[f]	42 (3)[f]
$Cu^+(MeOH)_4$	97.6 (1.2)	1.0 (0.1)	0.78 (0.04)	0.73 (0.02)	0.05	65 (5)
	99.4 (2.3)[f]	1.2 (0.1)[f]	0.77 (0.03)[f]	0.69 (0.02)[f]	0.08[f]	58 (5)[f]
$Cu^+(MeOH)_5$	85.9 (2.5)	1.0 (0.1)	0.93 (0.03)	0.72 (0.02)	0.21	30 (5)
	68.8 (2.5)[f]	1.7 (0.1)[f]	0.84 (0.04)[f]	0.51 (0.05)[f]	0.33[f]	32 (4)[f]
$Cu^+(MeOH)_6$	98.9 (5.2)[g]	1.5 (0.1)[g]	0.82 (0.02)[g]	0.26 (0.06)[g]	0.56[g]	25 (5)[g]
	97.1 (4.8)[f,g]	1.4 (0.1)[f,g]	0.86 (0.03)[f,g]	0.31 (0.03)[f,g]	0.55[f,g]	24 (4)[f,g]
	90.4 (1.3)[h]	1.5 (0.1)[h]	0.88 (0.03)[h]	0.18 (0.02)[h]	0.70[h]	23 (6)[h]
	90.5 (1.0)[f,h]	1.3 (0.1)[f,h]	0.90 (0.03)[f,h]	0.20 (0.18)[f,h]	0.70[f,h]	23 (5)[f,h]
	90.4 (1.9)[i]	1.5 (0.1)[i]	0.87 (0.03)[i]	0.18 (0.02)[i]	0.69[i]	24 (5)[i]
	89.9 (1.6)[f,i]	1.3 (0.1)[f,i]	0.89 (0.03)[f,i]	0.20 (0.15)[f,i]	0.69[f,i]	23 (5)[f,i]

[a] Uncertainties are listed in parenthesis. [b] Average values for a loose PSL transition state. [c] No RRKM analysis. [d] With RRKM analysis. Unless otherwise noted, the dissociation is assumed to occur from the ground-state reactant $Cu^+(MeOH)_x$ complex to the ground-state $Cu^+(MeOH)_{x-1}$ and MeOH products. [e] Difference between E_0 and E_0(PSL). [f] Average values obtained for fits to the total cross section. [g] Average values obtained for fits assuming that the reactant complex corresponds to the ground-state $Cu^+(MeOH)_{2,2,2}$ structure. [h] Average values obtained for fits assuming that the reactant complex corresponds to the $Cu^+(MeOH)_{2,2,1,1}$ structure. [i] Average values obtained for fits assuming that the reactant complex corresponds to the $Cu^+(MeOH)_{2,1,1,1,1}$ structure.

and higher-order products are more sensitive to lifetime and pressure effects,[51,70] and additional assumptions are needed to quantitatively include the multiple products formed. In addition, several low-energy conformers of the $Cu^+(MeOH)_6$ complex may be accessed in our experiments. Therefore, analyses of the CID cross sections for this system were performed using the molecular parameters associated with each of the three low-energy conformers dissociating to lose the most weakly bound MeOH molecule. The results of these analyses are provided in Table 1. However, for the largest $Cu^+(MeOH)_x$ complexes, that is, $x = 3-6$, the primary dissociation pathway is strongly affected by subsequent dissociation shortly after the threshold, such that the unaffected energy range is narrow. As a result, fits of the total cross section were also performed and were able to reproduce the data over a much broader energy range with good fidelity. The results of these analyses are also provided in Table 1.

Zero-pressure-extrapolated cross sections and fits to the data using a loose PSL model are shown in Figure 2 for loss of a single MeOH molecule from all six $Cu^+(MeOH)_x$ complexes arising from interaction with Xe (reaction 2), while fits to the total cross sections for the $Cu^+(MeOH)_x$, where $x = 3-6$, are shown in Figure 3. As can be seen in the figures, the cross sections are accurately reproduced using a loose PSL TS model. Previous work has shown that this model provides the most accurate assessment of the kinetic shifts for CID processes for electrostatically bound ion−molecule complexes.[44−54] Good reproduction of the data is obtained over energy ranges exceeding 3.5 eV and cross section magnitudes of at least a factor of 100. For the $x = 3-6$ complexes, the cross sections are finite at the lowest energies examined, and hence, the reproduction does not cover quite the same magnitude range.

Two threshold values E_0 and E_0(PSL) are listed in Table 1 for each analysis of each complex. E_0 represents the threshold obtained for analyses that do not include RRKM lifetime effects, whereas E_0(PSL) represents the threshold obtained when the RRKM lifetime analysis is included. Comparison of E_0 and E_0(PSL) threshold values shows that the rate of unimolecular dissociation, and therefore the kinetic shifts observed, depends both upon the threshold energy and the number of MeOH molecules surrounding the copper ion. The total number of vibrational modes increases with the size of the complex from 15 for $Cu^+(MeOH)$ to 105 for $Cu^+(MeOH)_6$. Similarly, the number of heavy atoms increases with the size of the complex from 3 for $Cu^+(MeOH)$ to 13 for $Cu^+(MeOH)_6$. Therefore, the densities of states of the dissociating complexes increase with size. The density of states also increases with collision energy. The measured thresholds for the $Cu^+(MeOH)$ and $Cu^+(MeOH)_2$ complexes are large and fairly similar, while the measured thresholds for the larger complexes are much smaller and decrease with increasing size of the complex. Thus, the kinetic shifts increase with increasing size of the complexes, except for the $Cu^+(MeOH)_3$ complex, which exhibits a smaller kinetic shift than that observed for the $Cu^+(MeOH)_2$ complex as a result of the much weaker binding in the former; see Table 1.

The entropy of activation, $\Delta S^\dagger$, is a measure of the looseness of the TS and also a reflection of the complexity of the system. It is determined from the molecular parameters used to model the energized molecule and the TS for dissociation but also depends upon the threshold energy. Listed in Table 1, the $\Delta S^\dagger$(PSL) values at 1000 K vary between 24 and 65 J K^{-1} mol^{-1} for the $Cu^+(MeOH)_x$ complexes examined here. The entropies of activation for these complexes compare favorably to a wide variety of noncovalently bound complexes previously measured in our laboratory.

Theoretical Results. Optimized geometries for neutral MeOH and the $Cu^+(MeOH)_x$ complexes were calculated using Gaussian 98, as described in the Theoretical Calculations section. BDEs calculated at the B3LYP/6-311+G(2d,2p)//B3LYP/6-31G* level of theory for the ground-state conformations of $Cu^+(MeOH)_x$, where $x = 1-5$, and for the three most stable conformations of the $Cu^+(MeOH)_6$ complex are listed in Table 2. Independent ZPE and BSSE corrections are made for all complexes. The B3LYP-optimized structures of the ground-state conformations for the $Cu^+(MeOH)_x$ complexes, $x = 1-6$, are shown in Figure 4. The B3LYP-optimized structures of all stable conformations of the $Cu^+(MeOH)_x$ complexes computed in this work are shown in Figure 1S of the Supporting Information. The relative stabilities of the various conformations of each $Cu^+(MeOH)_x$ complex determined at the B3LYP/6-311+G(2d,2p) level of theory including ZPE corrections are also included in the figure. Key geometrical parameters of the ground-state conformations of $Cu^+(MeOH)_x$, where $x = 1-5$, and for the three most stable conformations of the $Cu^+(MeOH)_6$ complex are summarized in Table 3. Parameters for all other stable low-energy excited conformations of the $Cu^+(MeOH)_x$ complexes are provided in the Supporting Information in Figure 1S.

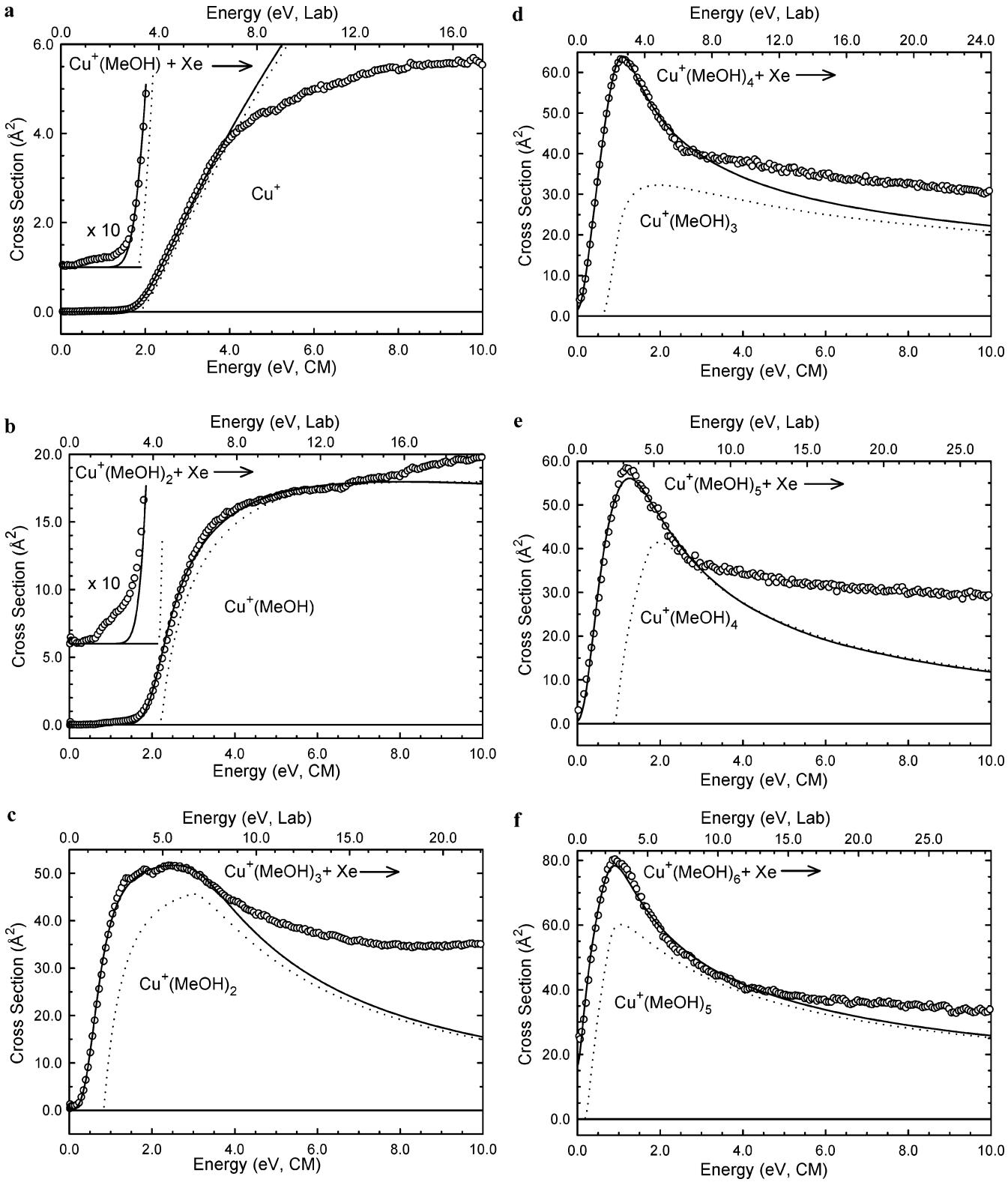

Figure 2. Zero-pressure-extrapolated primary product cross sections for CID of the $Cu^+(MeOH)_x$ complexes, where $x = 1-6$, with Xe in the threshold region as a function of kinetic energy in the center-of-mass frame (lower x axis) and laboratory frame (upper x axis), parts a through f, respectively. The solid lines show the best fit to the data using eq 1 convoluted over the ion kinetic and internal energy distributions. The dashed lines show the model cross sections in the absence of experimental kinetic energy broadening for reactants at 0 K.

Stable structures are found for the $Cu^+(MeOH)_x$ complexes, where $x = 1-4$, in which the arrangement of the oxygen donor atoms of the MeOH molecules around Cu^+ exhibits similarities to the ideal geometries predicted by the valence shell electron pair repulsion (VSEPR) model, that is, linear for $x = 1$ and 2, trigonal planar for $x = 3$, and tetrahedral for $x = 4$.[74] However, the theoretical calculations indicate that the $Cu^+(MeOH)_x$ complexes are more stable when the third, fourth, fifth, and sixth MeOH ligands are placed in the second and or third solvent shells and are hydrogen bonded to the MeOH molecules in the first or second solvent shell rather than directly bound to the copper ion. In the $Cu^+(MeOH)_x$ complexes, the distortion of

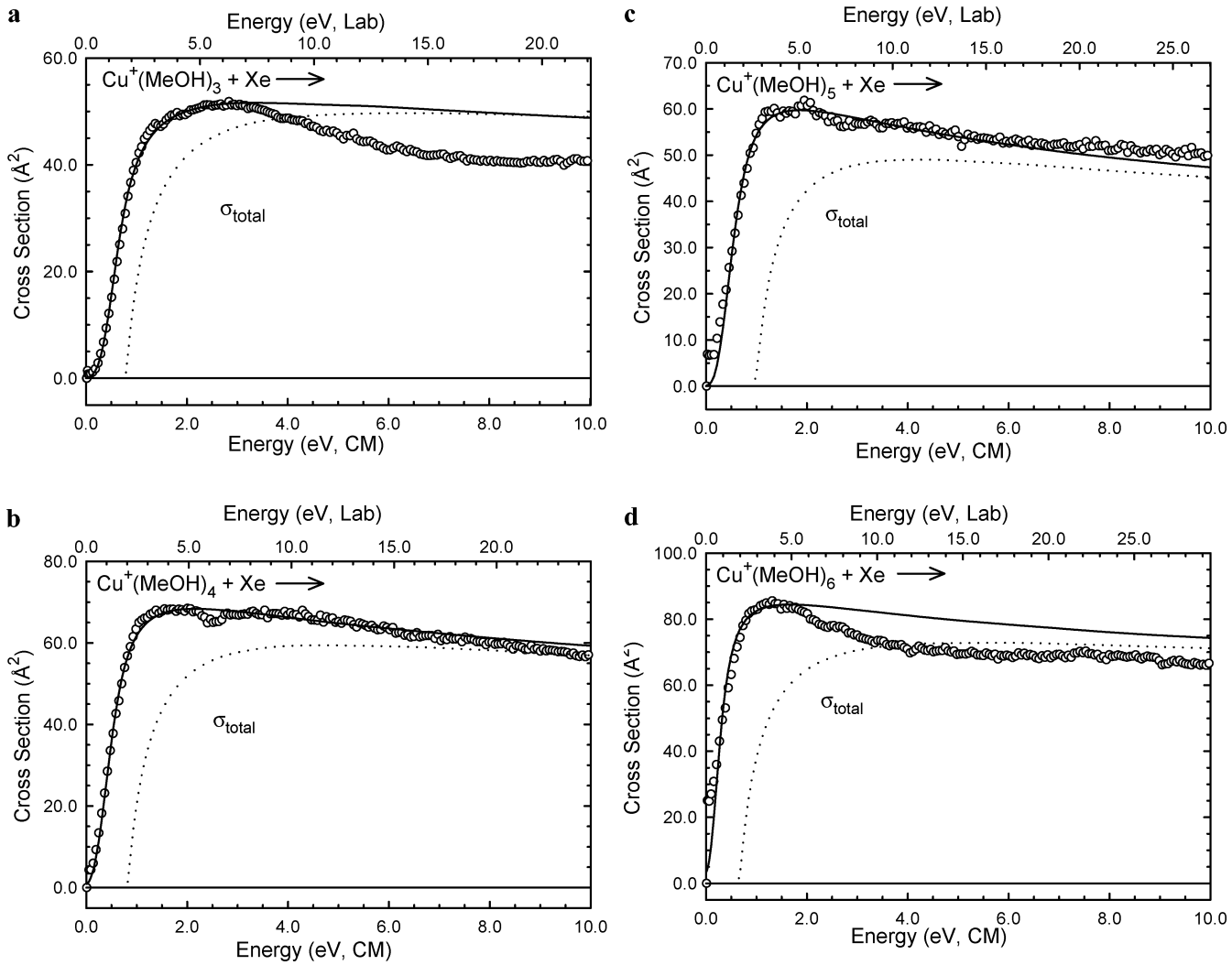

Figure 3. Zero-pressure-extrapolated total product cross sections for CID of the $Cu^+(MeOH)_x$, where $x = 3-6$, with Xe in the threshold region as a function of kinetic energy in the center-of-mass frame (lower *x* axis) and laboratory frame (upper *x* axis), parts a through d, respectively. The solid lines show the best fit to the data using eq 1 convoluted over the ion kinetic and internal energy distributions. The dashed lines show the model cross sections in the absence of experimental kinetic energy broadening for reactants at 0 K.

TABLE 2: Measured and Calculated Bond Dissociation Energies of $Cu^+(MeOH)_x$, $x = 1-6$, at 0 K in kJ/mol

complex	experiment TCID[a]	theory			
		CID	reaction	D_0[b]	$D_{0,BSSE}$[b,c]
$Cu^+(MeOH)$	178.3 (3.6)	1	→ 0	170.8	168.1
$Cu^+(MeOH)_2$	187.1 (2.5)	2	→ 1	180.4	176.5
$Cu^+(MeOH)_3$	72.8 (2.9)	2,1	→ 2	65.6	63.2
$Cu^+(MeOH)_4$	66.3 (2.0)	2,2	→ 2,1	60.9	58.7
$Cu^+(MeOH)_5$	49.7 (4.8)	2,2,1	→ 2,2	39.6	36.4
$Cu^+(MeOH)_6$	29.9 (3.2)	2,2,2	→ 2,2,1	37.2	35.0
		2,2,1,1	→ 2,2,1	34.3	32.1
		2,1,1,1,1	→ 2,1,1,1	28.6	26.5

[a] Present results, threshold collision-induced dissociation. [b] Calculated at the B3LYP/6−311+G(2d,2p)// B3LYP/6-31G* level of theory including ZPE corrections with B3LYP/6-31G* frequencies scaled by 0.9804. [c] Also includes BSSE corrections.

the MeOH molecule that occurs upon binding to Cu^+ is minor. The change in geometry is largest for the smallest complex, $Cu^+(MeOH)$, and decreases with increasing ligation.

$Cu^+(MeOH)$. A single stable structure is found for the $Cu^+(MeOH)$ complex (Figure 4). Cu^+ directly binds to the oxygen atom of MeOH with a Cu^+-O bond length of 1.780 Å and $\angle Cu^+OC$ bond angle of 122.0°, Table 3. The Cu^+-MeOH binding interaction is quite strong, 168.1 kJ/mol, Table 2.

$Cu^+(MeOH)_2$. Two stable conformations are found. In the ground-state structure (Figure 4), both MeOH ligands bind directly to the copper ion, with Cu^+-O bond lengths of 1.810 Å and $\angle Cu^+OC$ bond angles of 125.3°. The slightly longer Cu^+-O bond lengths and larger $\angle Cu^+OC$ bond angles are likely the result of repulsive ligand−ligand interactions in this complex. The orientation of the MeOH molecules is nearly antiparallel, such that the $\angle OCu^+O$ bond angle is nearly linear, 175.5°. This orientation minimizes ligand−ligand repulsion and maximizes stabilization via sd hybridization, as discussed below. Given the slightly longer Cu^+-O bond lengths, it is somewhat surprising that the second MeOH molecule is more strongly bound than the first, 176.5 kJ/mol, or 8.4 kJ/mol more strongly bound. This likely arises because the energetic cost associated with sd hybridization of Cu^+ is paid upon binding of the first MeOH molecule.

A stable hydrogen-bonded complex is also found (Figure 1S). This complex is designated as $Cu^+(MeOH)_{1,1}$ to indicate that one of the MeOH molecules binds directly to Cu^+ via interaction with the oxygen atom, thus occupying a site in the first solvent shell, while the second MeOH molecule binds to the MeOH

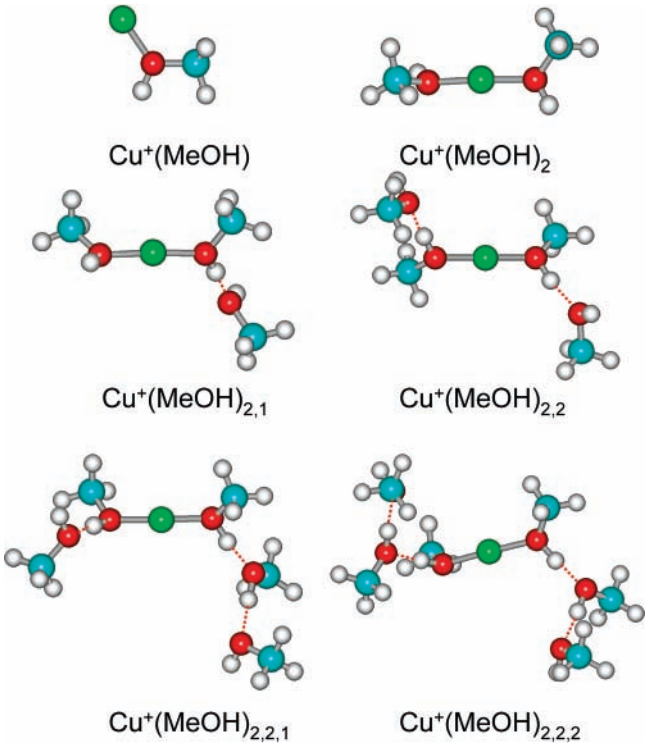

Figure 4. B3LYP/6-31G*-optimized geometries of ground-state conformations of $Cu^+(MeOH)_x$ complexes, where $x = 1-6$.

molecule in the first solvent shell via an O···H hydrogen bond and occupies a site in the second solvent shell. The ∠OHO bond angle is nearly linear, 174.1°, to provide maximal hydrogen-bond stabilization, while the backbones of the MeOH molecules are nearly perpendicular, such that the ∠COOC dihedral angle is 95.1°, to minimize ligand−ligand repulsion. This hydrogen-bonded complex, $Cu^+(MeOH)_{1,1}$, lies 103.4 kJ/mol higher in energy than the ground-state $Cu^+(MeOH)_2$ structure. Therefore, the second MeOH molecule prefers to bind directly to Cu^+ because the second Cu^+−MeOH interaction is significantly stronger than the O···H hydrogen bond.

$Cu^+(MeOH)_3$. Three low-energy conformations are found. In the ground-state structure, designated $Cu^+(MeOH)_{2,1}$ (Figure 4), two MeOH molecules bind directly to Cu^+, while the third MeOH molecule binds to one of the MeOH molecules in the first solvent shell via an O···H hydrogen bond and occupies a site in the second solvent shell. As in the $Cu^+(MeOH)_2$ and $Cu^+(MeOH)_{1,1}$ structures, the MeOH molecules are oriented to maximize stabilization via sd hybridization and minimize ligand−ligand repulsion.

In the next most stable conformation found, $Cu^+(MeOH)_3$, all three of the MeOH molecules bind directly to Cu^+. The orientation of the oxygen atoms of the MeOH molecules deviates from an idealized equilateral trigonal planar geometry, and instead, the ∠OCu^+O bond angles are 160.8, 110.4, and 88.9°, while the corresponding ∠COOC dihedrals angles are 1.0, 170.0, and 122.3°, respectively. Binding of the third MeOH molecule in the first solvent shell reduces stabilization gained via sd hybridization to a greater extent than binding in the second solvent shell. The T-shaped orientation of the MeOH molecules minimizes loss of stabilization via sd hybridization and ligand−ligand repulsion. This complex is found to lie 19.4 kJ/mol higher in energy than the ground-state structure, $Cu^+(MeOH)_{2,1}$.

In the third stable structure found, designated $Cu^+(MeOH)_{1,1,1}$ (Figure 1S), one of the MeOH molecules binds directly to Cu^+, while the second and third MeOH molecules occupy sites in the second and third solvent shells, respectively, and are bound to the inner MeOH molecules via O···H hydrogen bonds. This latter structure is found to be less stable than the ground-state structure by 122.3 kJ/mol. The relative stabilities of the stable conformations for this complex indicate that the first two Cu^+−MeOH interactions are significantly stronger than O···H hydrogen bonds, but beyond two MeOH molecules, O···H hydrogen bonds are more favorable.

$Cu^+(MeOH)_4$. Six low-energy conformations are found. In the ground-state structure, designated $Cu^+(MeOH)_{2,2}$ (Figure 4), the first two MeOH molecules bind directly to Cu^+, while the third and fourth MeOH molecules each bind to one of the MeOH molecules in the first solvent shell via O···H hydrogen bonds and occupy sites in the second solvent shell. The relative orientations of the MeOH molecules in the first and second solvent shell parallel that found for the ground-state conformations of the smaller complexes.

The structure designated as $Cu^+(MeOH)_{2,1,1}$ is the next most stable structure found and lies 20.4 kJ/mol above the ground-state conformer (Figure 1S). In this structure, the first two MeOH molecules bind directly to Cu^+, the third MeOH molecule binds to one of the MeOH molecules in the first solvent shell via an O···H hydrogen bond and occupies a site in the second solvent shell, while the fourth MeOH molecule binds to this latter MeOH molecule via an O···H hydrogen bond and occupies a site in the third solvent shell.

The structure designated as $Cu^+(MeOH)_{3,1A}$ is the next most stable structure found and lies 25.7 kJ/mol above the ground-state conformer (Figure 1S). In this structure, the first three MeOH molecules bind directly to Cu^+ and occupy sites in the first solvent shell, while the fourth MeOH molecule is bound to two of the inner-shell MeOH molecules via O···H hydrogen bonds and occupies a site in the second solvent shell. A similar structure, designated as $Cu^+(MeOH)_{3,1B}$, is the next most stable found and lies 29.6 kJ/mol above the ground-state conformer (Figure 1S). In this structure, the first three MeOH molecules are again directly bound to Cu^+, while the fourth MeOH molecule is bound to only one of the inner-shell MeOH molecules via a single O···H hydrogen bond. The small difference in the stabilities of these $Cu^+(MeOH)_{3,1}$ complexes indicates that the stabilization gained via the second hydrogen bonding interaction is almost completely consumed by the energetic cost associated with the structural changes necessary to accommodate both hydrogen-bonding interactions.

The next most stable structure found lies 53.8 kJ/mol above the ground state and is designated $Cu^+(MeOH)_4$ (Figure 1S). In this structure, all four MeOH molecules bind directly to Cu^+ in a nearly tetrahedral arrangement of the oxygen donor atoms around Cu^+. Clearly, the loss of stabilization via sd hybridization and increased ligand−ligand repulsion make this a much less favorable geometry for binding.

The least stable binding conformation computed is designated $Cu^+(MeOH)_{1,1,1,1}$ (Figure 1S). In this structure, one of the MeOH molecules binds directly to Cu^+, while the second, third, and fourth MeOH molecules occupy sites in the second, third, and fourth solvent shells, respectively, and are bound to the inner MeOH molecules via O···H hydrogen bonds. This latter structure is found to be less stable than the ground-state structure by 145.7 kJ/mol. The relative stabilities of the various stable conformations of $Cu^+(MeOH)_4$ again indicate that the first two Cu^+−MeOH interactions are significantly stronger than O···H hydrogen bonds, while O···H hydrogen-bonding interactions are favored beyond two MeOH ligands directly interacting with Cu^+.

TABLE 3: Geometrical Parameters of the B3LYP/6-31G* Geometry-Optimized Ground-State Structures of $Cu^+(MeOH)_x$ Complexes, $x = 1-6$, and Low-Energy Structures for $x = 6$

	bond length (Å)		bond angle (°)	
species	Cu^+-O	H···OH	∠OCu⁺O	∠Cu⁺OC
$Cu^+(MeOH)$	1.780	–	–	122.0
$Cu^+(MeOH)_2$	1.810	–	175.5	125.3
	1.810			125.3
$Cu^+(MeOH)_{2,1}$	1.822	1.591	176.3	123.1
	1.803			124.5
$Cu^+(MeOH)_{2,2}$	1.808	1.607	176.6	122.7
	1.807	1.613		122.7
$Cu^+(MeOH)_{2,2,1}$	1.802	1.525, 1.718	175.1	121.8
	1.812	1.617		119.7
$Cu^+(MeOH)_{2,2,2}$	1.804	1.537, 1.534	175.1	121.5
	1.807	1.727, 1.723		118.6
$Cu^+(MeOH)_{2,2,1,1}$	1.802	1.491, 1.649, 1.757		123.0
	1.810	1.624		118.4
$Cu^+(MeOH)_{2,1,1,1,1}$	1.795	1.480, 1.645, 1.685, 1.764		123.6
	1.827			119.2

[a] H···OH bond lengths are listed in order of increasing distance from Cu^+ for each of the two Cu^+-MeOH interaction chains.

$Cu^+(MeOH)_5$. Six low-energy conformers are found. In the ground-state structure, designated $Cu^+(MeOH)_{2,2,1}$ (Figure 4), the first two MeOH molecules bind directly to Cu^+, the third and fourth MeOH molecules each bind to one of the MeOH molecules in the first solvent shell via O···H hydrogen bonds, thus occupying sites in the second solvent shell, and the fifth MeOH molecule binds to one of the MeOH molecules in the second solvent shell via an O···H hydrogen bond, thus occupying a site in the third solvent shell. The relative stabilities of the other low-energy structures parallel that found for the smaller complexes (compare Figures 4 and 1S).

$Cu^+(MeOH)_6$. Nine low-energy conformers are found. In the ground-state conformation, designated $Cu^+(MeOH)_{2,2,2}$ (Figure 1S), the first two MeOH molecules bind directly to Cu^+, the third and fourth MeOH molecules each bind to one of the MeOH molecules in the first solvent shell via O···H hydrogen bonds occupying sites in the second solvent shell, while the fifth and sixth MeOH molecules bind to the MeOH molecules in the second solvent shell via O···H hydrogen bonds and occupy sites in the third solvent shell. The relative stabilities of the other stable conformers again parallel that found for the smaller complexes (Figures 4 and 1S).

Comparison of all of the stable structures computed and their relative stabilities indicates that the most favorable binding is achieved when only two of the MeOH molecules bind directly to Cu^+. The remaining MeOH molecules then bind to the $Cu^+(MeOH)_2$ core via hydrogen-bonding interactions. The hydrogen-bonding interactions become progressively weaker as the MeOH molecules occupy sites further from Cu^+, indicating that the inner MeOH molecules effectively shield the charge. The binding becomes increasingly less favorable as the number of MeOH molecules directly binding to Cu^+ increases beyond two. However, the least favorable binding is observed for complexes in which only one MeOH molecule binds directly to Cu^+. Among the various conformations having an equivalent number of MeOH molecules directly bound to Cu^+, the relative stabilities are determined by the number and location of the hydrogen bonds (i.e., the more hydrogen bonds and the closer they are to the Cu^+ center, the more stable the structure).

NBO Analyses. NBO analyses were performed for the ground-state and several low-lying excited conformations of the $Cu^+(MeOH)_x$ complexes. The corresponding $E(2)$ stabilization energies were obtained between the electron donor and acceptor orbitals. The dominant donor−acceptor interactions are summarized in Table 4. The NBO analyses reveal that the binding in these complexes is dominated by two types of donor−acceptor interactions. The first type of interaction arises when a MeOH molecule occupies a site in the first solvation shell and interacts directly with Cu^+ such that binding occurs via ligand-to-metal σ donation of the lone pair of electrons of the oxygen atom to an unoccupied orbital on Cu^+, LP(O) → L*(Cu). Additional minor ligand-to-metal σ donor interactions, where electron density from the O−H and C−O bonds is donated to an unoccupied orbital on Cu^+, BD(O−H) → LP*(Cu) and BD(C−O) → LP*(Cu), also contribute to the binding in these complexes but contribute less than 20% of the total stabilization energy. The second type of interaction arises when a MeOH molecule occupies a site in an outer solvation shell and hydrogen bonds to another MeOH molecule in an inner shell such that the binding occurs via σ donation from the lone pair of electrons of the oxygen atom of the outer MeOH to the antibonding orbital of the hydroxyl group of the inner MeOH, LP(O) → BD*(O−H). These outer-shell MeOH molecules also interact with Cu^+ via a long-range interaction that is screened by the inner MeOH molecule(s). However, the NBO analyses indicate that very little stabilization (i.e., less than 2 kJ/mol) is gained via such long-range interactions, likely a result of the local nature of the NBO analyses. It is not surprising that very little stabilization (2−7% of the total stabilization energy) is gained via metal-to-ligand back-donation interactions because MeOH is not a very effective π acceptor ligand.

The NBO analyses also provide valuable information about the hybridization of Cu^+ in these complexes. For example, the ground-state electron configuration of isolated Cu^+ is $4s^0 3d^{10}$. The natural electron configurations of Cu^+ in the $Cu^+(MeOH)_x$ complexes for which NBO analyses were performed are also summarized in Table 4 and clearly show that the 4s and 3d orbitals of Cu^+ in these complexes are hybridized to help minimize Pauli repulsion between Cu^+ and the MeOH ligand(s) but that the extent of hybridization varies with the number of MeOH ligands in the first solvent shell that are directly interacting with the Cu^+ ion. As can be seen in the table, all complexes with two MeOH ligands in the first solvent shell have very similar Cu^+ electron configurations with greater occupation of the 4s orbital and greater total electron occupation than those with one, three, or four MeOH ligands in the first solvent shell. The increased electron occupation of Cu^+ in the complexes where two MeOH ligands occupy sites in the first

TABLE 4: Second-Order Perturbation Energies $E(2)$ Corresponding to the Dominant Charge-Transfer Interactions (Donor → Acceptor) of Ground-State and Selected Low-Lying Excited Conformations of the $Cu^+(MeOH)_x$ Complexes, Where $x = 1-6$[a]

species	Cu^+ e^- configuration	donor NBO	acceptor NBO	$E(2)$ energy (kJ/mol)
$Cu^+(MeOH)$	$4s^{0.45}3d^{9.63}4p^{0.02}5p^{0.02}$	LP(O)	LP*(Cu)	203.6
$Cu^+(MeOH)_2$	$4s^{0.68}3d^{9.51}4p^{0.02}$	LP(O)	LP*(Cu)	254.1 (2)
$Cu^+(MeOH)_{2,1}$	$4s^{0.71}3d^{9.50}4p^{0.02}$	LP(O)	LP*(Cu)	276.7, 255.4
		LP(O)	BD*(O−H)	167.3
$Cu^+(MeOH)_3$	$4s^{0.53}3d^{9.58}4p^{0.05}$	LP(O)	LP*(Cu)	202.6 (2), 51.2
$Cu^+(MeOH)_{2,2}$	$4s^{0.73}3d^{9.49}4p^{0.02}$	LP(O)	LP*(Cu)	274.3 (s)
		LP(O)	BD*(O−H)	157.7 (2)
$Cu^+(MeOH)_{3,1A}$	$4s^{0.50}3d^{9.59}4p^{0.08}$	LP(O)	LP*(Cu)	188.9 (2), 62.7
		LP(O)	BD*(O−H)	84.7, 51.1
$Cu^+(MeOH)_{3,1B}$	$4s^{0.57}3d^{9.56}4p^{0.05}$	LP(O)	LP*(Cu)	228.9, 197.5, 44.3
		LP(O)	BD*(O−H)	130.2
$Cu^+(MeOH)_4$	$4s^{0.37}3d^{9.66}4p^{0.10}$	LP(O)	LP*(Cu)	134.9 (2), 53.3 (2)
$Cu^+(MeOH)_{2,2,1}$	$4s^{0.74}3d^{9.48}4p^{0.04}$	LP(O)	LP*(Cu)	329.9, 311.8
		LP(O)	BD*(O−H)	398.0, 287.7, 177.4
$Cu^+(MeOH)_{2,2,2}$	$4s^{0.75}3d^{9.47}4p^{0.04}$	LP(O)	LP*(Cu)	329.4 (2)
		LP(O)	BD*(O−H)	458.3 (2), 231.9 (2)

[a] Only $E(2)$ stabilization energies for the dominant interactions are shown. Average values are reported when multiple interactions are of very similar energies. In such cases, degeneracies are provided in parentheses. The orbital designations are defined as "LP" for one-center valence lone pairs, LP* for one-center empty non-Lewis NBO, and "BD*" for two-center antibonding orbitals.

TABLE 5: Enthalpies and Free Energies of Ground-State $Cu^+(MeOH)_x$ and Low-Lying $Cu^+(MeOH)_6$ Complexes, $x = 1-6$, at 298 K in kJ/mol[a]

complex	ΔH_0	$\Delta H_0{}^b$	$\Delta H_{298} - \Delta H_0{}^b$	ΔH_{298}	$\Delta H_{298}{}^b$	$T\Delta S_{298}{}^b$	ΔG_{298}	$\Delta G_{298}{}^b$
$Cu^+(MeOH)$	178.3 (3.6)	168.1	2.4 (0.2)	180.7 (3.6)	170.5	28.1 (0.4)	152.6 (3.6)	142.4
$Cu^+(MeOH)_2$	187.1 (2.5)	176.5	0.2 (0.3)	187.3 (2.5)	176.7	42.5 (1.1)	144.8 (2.7)	134.2
$Cu^+(MeOH)_3$	72.8 (2.9)	63.2	1.5 (0.4)	74.3 (2.9)	64.7	41.8 (1.4)	32.5 (2.9)	22.9
$Cu^+(MeOH)_4$	66.3 (2.0)	58.7	0.1 (0.3)	66.4 (2.0)	58.8	44.6 (1.1)	21.8 (2.3)	14.2
$Cu^+(MeOH)_5$	49.7 (4.8)	36.4	1.7 (0.2)	51.4 (4.8)	38.1	38.7 (1.2)	12.7 (4.9)	−0.6
$Cu^+(MeOH)_6$	29.9 (3.2)	35.0	0.6 (0.2)	30.5 (3.2)	35.6	35.6 (1.1)	−5.1 (3.4)	0
$Cu^+(MeOH)_6$	19.3 (1.7)	32.1	−2.4 (1.2)	16.9 (2.1)	29.7	30.6 (5.7)	−13.7 (6.1)	−0.9
$Cu^+(MeOH)_6$	19.2 (1.4)	26.5	−1.6 (1.3)	17.6 (1.9)	24.9	36.7 (5.3)	−19.1 (5.6)	−11.8

[a] Uncertainties are listed in the parentheses and determined as described in the text. [b] Density functional theory values from calculations at the B3LYP/6-311+G(2d,2p)//B3LYP/6-31G* level of theory with frequencies scaled by 0.9804. [c] Values for the ground-state conformer, $Cu^+(MeOH)_{2,2,2}$, dissociating to $Cu^+(MeOH)_{2,2,1}$ + MeOH. [d] Values for the $Cu^+(MeOH)_{2,2,1,1}$ conformer dissociating to $Cu^+(MeOH)_{2,2,1}$ + MeOH. [e] Values for the $Cu^+(MeOH)_{2,1,1,1,1}$ conformer dissociating to $Cu^+(MeOH)_{2,1,1,1}$ + MeOH.

solvent shell indicates stronger binding, in agreement with the relative stabilities computed for these $Cu^+(MeOH)_x$ complexes. A single MeOH ligand is not able to donate as much electron density to Cu^+ due to the single interaction, while more than two MeOH ligands are not able to donate as much electron density to Cu^+ because the third (and fourth) MeOH ligands experience greater repulsion with the occupied sd hybrid orbital. Thus, both environments lead to weaker binding than when only two MeOH ligands interact directly with Cu^+, in agreement with the computed relative stabilities of these complexes.

Conversion from 0 to 298 K. To allow comparison to commonly used experimental conditions, we convert the 0 K BDEs determined here (experimentally and theoretically) to 298 K bond enthalpies and free energies. The enthalpy and entropy conversions are calculated using standard formulas (assuming harmonic oscillator and rigid rotor models) and the vibrational and rotational constants determined for the B3LYP/6-31G*-optimized geometries. Table 5 lists 0 and 298 K enthalpy, free energy, and enthalpic and entropic corrections for all systems experimentally determined. Uncertainties in the enthalpic and entropic corrections are determined by 10% variation in the molecular constants (vibrational frequencies and rotational constants). Because theory may not adequately describe the weak interactions in these systems, the listed uncertainties also include contributions from scaling all frequencies below 150 cm^{-1} up and down by a factor of 2. The latter provides a conservative estimate of the computational errors in these low-frequency modes and is the dominant source of the uncertainties listed.

Discussion

Comparison of Theory and Experiment. The sequential BDEs for the $Cu^+(MeOH)_x$ complexes, where $x = 1-6$, at 0 K measured here by threshold collision-induced dissociation (TCID) techniques in a guided ion beam tandem mass spectrometer are summarized in Table 2. Also listed here are the 0 K BDEs calculated at the B3LYP/6-311+G(2d,2p)//B3LYP/6-31G* level of theory, including ZPE and BSSE corrections. The agreement between the TCID-measured BDEs and those calculated at the B3LYP/6-311+G(2d,2p) level of theory (including and excluding BSSE corrections) is illustrated in Figure 5 and is quite good for all complexes. The mean absolute deviation (MAD) between the experimentally measured BDEs and those calculated for the ground-state conformations of all six $Cu^+(MeOH)_x$ complexes is 9.4 ± 2.8 kJ/mol when BSSE corrections are included and reduces to 7.9 ± 1.9 kJ/mol when BSSE corrections are not included. This is not surprising considering that the ions generated under our experimental conditions have internal energies that are well described by a Maxwell−Boltzmann distribution at room temperature. Thus, the relative populations of the ground-state $Cu^+(MeOH)_x$ conformers, $x = 1-5$, are significantly larger (>99.9%) than those of all other corresponding low-energy conformers. However, for the $Cu^+(MeOH)_6$ complexes, multiple low-energy conformers were found that lie within 10 kJ/mol of the ground-state geometry. It is possible that several other low-energy conformers also exist and are populated under our experimental conditions. It should be noted that the TCID technique is a

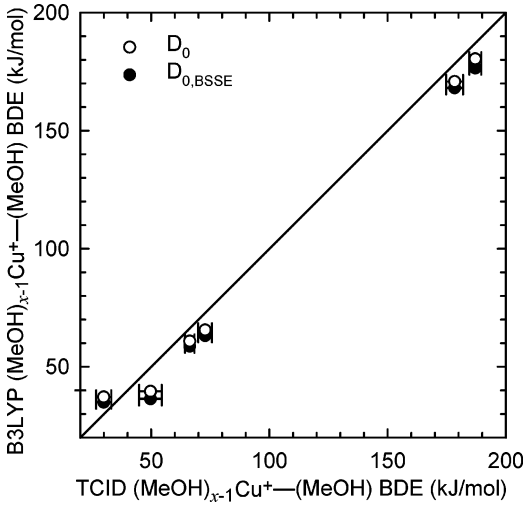

Figure 5. Comparison of the TCID-measured and B3LYP-calculated $(MeOH)_{x-1}Cu^+-MeOH$ BDEs at 0 K (in kJ/mol), where $x = 1-6$. The theoretical BDES computed when BSSE corrections are not included are shown as ●, while values that included BSSE corrections are shown as ○.

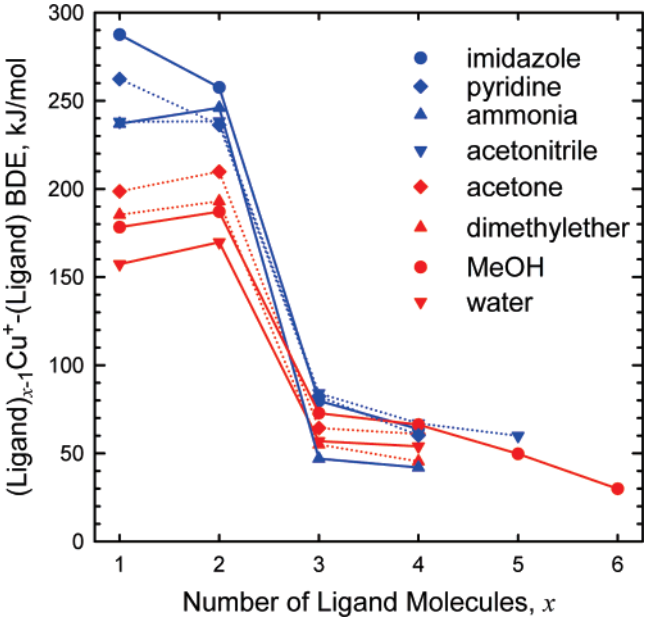

Figure 6. Experimental and theoretical $(ligand)_{x-1}Cu^+-ligand$ BDEs at 0 K (in kJ/mol) plotted versus the number of ligands *x*. Values are taken from ref 39 for H_2O (▽), ref 45 for CH_3CN (▼), ref 43 for CH_3OCH_3 (△), ref 48 for imidazole (●), ref 44 for NH_3 (▲), and ref 46 for CH_3COCH_3 (○).

threshold technique, and therefore, the thermochemistry derived from such studies is only sensitive to the lowest-energy dissociation pathway available. Therefore, the measured threshold only provides the BDE of the $Cu^+(MeOH)_6$ complex that is the most weakly bound and present in reasonable abundance (i.e., at least a few percent or is a weighted average of those present in reasonable abundance if close in energy). Thus, if either of the $Cu^+(MeOH)_{2,2,1,1}$ or $Cu^+(MeOH)_{2,1,1,1,1}$ or other low-energy excited conformers are formed under our experimental conditions, the calculated BDEs of 32.1 and 26.5 kJ/mol, respectively, agree better with the experimental result, 29.9 ± 3.2 kJ/mol. Given the good agreement between experiment and theory for $x = 1-5$, this suggests that we do indeed form multiple low-energy conformers of $Cu^+(MeOH)_6$ under our experimental conditions. Further support for this conclusion comes from the observation that the theoretical values are consistently lower than the measured BDEs for the $Cu^+(MeOH)_x$, $x = 1-5$, complexes but greater than the BDE measured for $Cu^+(MeOH)_{2,2,2}$. The actual structure of the most weakly bound $Cu^+(MeOH)_6$ complexes accessed in our experiments is not known but is likely to be similar to that of the $Cu^+(MeOH)_{2,1,1,1,1}$ complex computed here.

Trends in the Sequential Bond Dissociation Energies of $Cu^+(MeOH)_x$ Complexes. The BDEs of $Cu^+(MeOH)_x$ complexes, where $x = 1$ and 2, are quite strong and increase somewhat from $x = 1$ to 2. A sharp decrease in the BDE occurs for $x = 3$, and then, fairly small decreases are observed as *x* varies from 3 to 6. Similar behavior has been observed for the solvation of Cu^+ by several other ligands, for example, water,[37−41] ammonia,[42] acetonitrile,[45] acetone,[46] dimethylether,[47] imidazole,[48] and pyridine.[49] A comparison of the trends in the sequential BDEs of Cu^+ to MeOH and the above ligands is shown in Figure 6. As can be seen in the figure, the trends in the sequential BDEs for all of these $Cu^+(ligand)_x$ complexes are very similar: very strong binding of the first two ligands and significantly weaker binding of additional ligands. This behavior arises as a result of sd hybridization of Cu^+, which hybridizes electron density away from the ligand in a direction perpendicular to the bonding axis. This allows the first two ligands to approach Cu^+ with minimum electronic repulsion. The effects of sd hybridization continue to influence the larger $Cu^+(ligand)_x$ complexes because when additional ligands bind to Cu^+, they experience greater electronic repulsion with the occupied sd hybrid orbital. This leads to much weaker binding of additional ligands and also exerts a strong influence on the geometry of the larger complexes. In the case of MeOH, binding of additional MeOH ligands in the second and/or higher-order solvent shells reduces the electronic repulsion with the occupied sd hybrid orbital and, thereby, allows more of the stabilization gained via sd hybridization to be maintained while binding the MeOH molecule via a hydrogen bond and a longer-range electrostatic interaction with the copper ion. Such alternative hydrogen-bonding interactions are also possible for other ligands capable of simultaneously acting as both a hydrogen bond donor and acceptor, for example, water, ammonia, and imidazole. Thus, both the trends in the sequential BDEs and the stable geometries of the $Cu^+(ligand)_x$ complexes are dominated by effects associated with the sd hybridization of Cu^+. The highly parallel behavior across these $Cu^+(ligand)_x$ complexes suggests that the nature of the ligand plays a lesser role in determining the strength and geometries of binding.

Comparison to Other Ligands. As discussed above, the nature of the ligand plays only a minor role in determining the geometries and sequential BDEs of the $Cu^+(ligand)_x$ complexes. The binding in the $Cu^+(ligand)_x$ complexes is largely noncovalent and arises primarily from ion−dipole, ion-induced dipole, and hydrogen-bonding interactions in these complexes. However, it is often the case that one of these terms is dominant. Therefore, it is useful to compare the trends in the BDEs to the dipole moments and polarizabilities of the ligands. The N donor ligands bind more strongly to Cu^+ than O donor ligands, except for the $x = 3$ and 4 complexes to ammonia. Among the N donor ligands, the strength of the binding of the first ligand follows the order imidazole > pyridine > acetonitrile ≈ ammonia. This trend does not parallel either the dipole moments (3.96, 2.31, 3.92, and 1.47 D, respectively) or polarizabilities of these ligands (7.17, 9.25, 4.48, and 2.26 Å^3, respectively). Clearly, the smaller dipole moment of pyridine leads to weaker binding as compared to that of imidazole. However, the large polarizability of pyridine partially compensates and leads to stronger binding than to

acetonitrile. Among the O-containing ligands, binding follows the order of acetone > dimethyl ether > MeOH > water. This trend parallels the polarizability of these ligands (6.40, 5.15, 3.26, and 1.45 Å^3, respectively). However, this trend differs somewhat from the trend in the dipole moments for these ligands (2.88, 1.30, 1.74, and 1.85 D, respectively). This suggests that the much larger polarizabilities of dimethyl ether and MeOH compared to that of water overcome the smaller dipole moments.

The trends in the sequential BDEs of these $Cu^+(ligand)_x$ complexes can be understood in terms of a balance of several effects, the electrostatic ion−dipole attraction, sd hybridization of the orbitals of Cu^+, electron donor−acceptor NBO stabilization, and ligand−ligand repulsion. The electrostatic contribution to the binding can be expected to decrease upon ligation. This arises as a result of the decline in the effective positive charge retained by Cu^+ and the increasing repulsion between the ligands as the extent of ligation increases. However, the BDEs of $Cu^+(ligand)_x$ complexes, where $x = 1$ and 2, are much stronger than the more highly ligated complexes, that is, $Cu^+(ligand)_x$ ($x \geq 3$). Cu^+ is a $4s^03d^{10}$ ion, and therefore, the dσ orbital is occupied. This leads to greater Pauli repulsion between the copper ion and the ligand than when it is unoccupied. The sd hybridization of Cu^+ effectively removes electron density from the copper−ligand axis by placing electron density in a hybridized orbital that is perpendicular to the bonding axis. This allows the ligands to approach Cu^+ with lower repulsion energy. The BDEs of the second ligand are generally slightly stronger than those of the first ligand because the energetic cost associated with sd hybridization is paid upon binding of the first ligand, and the ligand−ligand repulsive interactions are typically weaker than the cost of sd hybridization.

The effects of sd hybridization lead to much weaker binding of additional ligands beyond the first two. If the stabilization gained via sd hybridization is almost completely lost when the third ligand binds directly to Cu^+, then equilateral trigonal planar and tetrahedral geometries are expected for the $Cu^+(ligand)_3$ and $Cu^+(ligand)_4$ complexes, respectively. Ligand−ligand repulsion also influences the BDEs and geometries of the multiply ligated complexes. The BDEs decrease with increasing ligation as the result of the decreasing positive charge retained by Cu^+ and increasing ligand−ligand repulsion. For example, our calculations find three different stable structures for the $Cu^+(MeOH)_3$ complexes (Figures 4 and 1S). In the $Cu^+(MeOH)_{2,1}$ structure, two MeOH molecules bind directly to Cu^+, while the third MeOH molecule occupies a site in the second solvation shell and binds to one of the first two MeOH molecules via an O···H hydrogen bond. In the $Cu^+(MeOH)_3$ structure, all three MeOH molecules bind directly to Cu^+, resulting in a trigonal planar geometry. In the $Cu^+(MeOH)_{1,1,1}$ structure, the first MeOH molecule binds directly to Cu^+, while the second and the third MeOH molecules occupy sites in the second and third solvation shells and bind via O···H hydrogen bonds. The $Cu^+(MeOH)_{2,1}$ structure is energetically more favorable because this arrangement does not disturb the sd hybridization of Cu^+ and experiences the least ligand−ligand repulsion. The $Cu^+(MeOH)_{1,1,1}$ structure is the least stable because the hydrogen bond between the MeOH molecules in the second and third solvation shells is much weaker than the Cu^+−O bonds in the $Cu^+(MeOH)_{2,1}$ and $Cu^+(MeOH)_3$ structures. In our previous studies of the $Cu^+(imidazole)_x$ and $Cu^+(pyridine)_x$ complexes, $x = 1-4$, ligand−ligand repulsion is even more significant such that the BDEs of the $Cu^+(imidazole)_2$ and $Cu^+(pyridine)_2$ complexes are lower than those of Cu^+(imidazole) and Cu^+(pyridine), respectively.[48,49] This likely arises because these ligands are much stronger field ligands than the other ligands compared here.

Stable hydrogen-bonded structures for the $Cu^+(ligand)_x$ complexes involving ligands occupying sites in the second (or larger) solvent shells are only available for ligands that possess both hydrogen bond donor and hydrogen bond acceptor groups, for example, ammonia, water, imidazole, and MeOH, whereas the hydrogen atoms on pyridine, acetonitrile, dimethyl ether, and acetone are not sufficiently acidic to provide good hydrogen-bonding sites. The ability to form such hydrogen-bonded structures clearly impacts both the structure and stability of the larger $Cu^+(ligand)_x$ complexes. However, the parallel behavior observed for the $Cu^+(ligand)_x$ complexes both capable and incapable of such hydrogen-bonding interactions suggests that these effects are much less important than the sd hybridization of Cu^+.

The relative BDEs of the $Cu^+(ligand)_x$ complexes will influence the composition of complexes of copper ions solvated by multiple ligands. For example, ammonia ligands bind more strongly than water in the Cu^+(ligand) and $Cu^+(ligand)_2$ complexes, Figure 6. Therefore, ammonia molecules always try to occupy the first solvent shell in mixed ammine−aqua complexes.[35] Similar behavior is expected for all N donor ligands as a result of their stronger binding to Cu^+. Because MeOH binds more strongly than water for the Cu^+(ligand) and $Cu^+(ligand)_2$ complexes, it is likely that MeOH would bind directly to the copper ion in the first solvent shell in mixed MeOH/water complexes, such as those that would be formed when a MeOH/water mixture is used for ESI experiments. Thus, knowledge of the thermochemistry of the various species in ESI solutions provides clues to the microstructures of the complexes of solvated metal ions and molecular ions in solution.

NBO Analyses. Further insight into the nature of the binding in these $Cu^+(MeOH)_x$ complexes can be extracted from the NBO analyses. Examination of the $E(2)$ stabilization energies for the dominant binding interactions in the $Cu^+(MeOH)_x$ complexes provides a more detailed understanding of the nature of the binding in these complexes (Table 4). The $E(2)$ stabilization energy computed for the LP(O) → LP*(Cu) interaction in Cu^+(MeOH) is 203.6 kJ/mol and increases to 254.1 kJ/mol for each LP(O) → LP*(Cu) interaction in $Cu^+(MeOH)_2$. This increase in stabilization is likely the result of the cost of sd hybridization having been paid upon binding of the first MeOH ligand. Binding of a third MeOH ligand directly to Cu^+ leads to geometric distortions such that the first two ligands are no longer oriented to take maximal advantage of sd hybridization effects, and the third MeOH ligand experiences very strong repulsion with the occupied sd hybrid orbital. As a result, the $E(2)$ stabilization energies associated with the binding of each of the first two ligands reduces to 202.6 kJ/mol, and that for the third Cu^+−MeOH interaction is much lower, 51.2 kJ/mol. The loss of stabilization arising from sd hybridization upon binding of additional ligands is even more severe for the $Cu^+(MeOH)_4$ complex, where the $E(2)$ stabilization energies are found to be even smaller, 134.9 kJ/mol each for the binding of the first and second MeOH ligands and 53.3 kJ/mol each for the binding of the third and fourth MeOH ligands.

Binding of additional MeOH molecules in the second and third solvent shells leads to greater stabilization because it minimizes the electronic repulsion with the occupied sd hybrid orbital. In addition, the hydrogen-bonding interaction induces polarization in the MeOH ligand to which it is hydrogen bound, leading to greater stabilization. This is easily seen by comparing the $E(2)$ stabilization energies of the $Cu^+(MeOH)_2$ and

$Cu^+(MeOH)_{2,1}$ complexes, where the $E(2)$ stabilization energy associated with the LP(O) → LP*(Cu) interaction increases from 254.1 to 276.7 kJ/mol upon binding of the third MeOH molecule in the second solvent shell. This strongly contrasts that found for the $Cu^+(MeOH)_3$ complex discussed above. Similar comparisons can be made for a variety of complex pairs that differ only by the presence of a single MeOH ligand that is hydrogen bound to the complex. When binding occurs in the third solvent shell, both inner MeOH ligands become polarized, thereby leading to increased $E(2)$ stabilization energies for both the LP(O) → LP*(Cu) and LP(O) → BD*(O−H) interactions (e.g., compare the $E(2)$ stabilization energies for the $Cu^+(MeOH)_2$, $Cu^+(MeOH)_{2,2}$, and $Cu^+(MeOH)_{2,2,2}$ complexes).

Overall, the absolute strength of the binding interactions becomes weaker as the $Cu^+(MeOH)_x$ complex becomes larger and as the MeOH ligand occupies a site more distant from the Cu^+ core of the complex (see Table 2). That is, the first two MeOH ligands are very strongly bound, the MeOH ligands occupying sites in the second solvent shells bind less strongly, and those occupying sites in the third solvent shell even less strongly, and so forth. Thus, hydrogen-bonding interactions become progressively weaker as a result of screening of the core charge by the inner MeOH molecules. This is not obvious from the $E(2)$ stabilization energies summarized in Table 4. However, it must be remembered that the NBO analyses compute local donor−acceptor stabilization interactions but do not compute destabilization interactions such as ligand−ligand repulsive interactions, which increase with the size of the complex.

Conclusions

The kinetic energy dependences of the collision-induced dissociation of $Cu^+(MeOH)_x$, $x = 1-6$, with Xe are examined in a guided ion beam mass spectrometer. The dominant dissociation processes for all complexes is the sequential loss of intact MeOH molecules. From the thresholds for the primary dissociation processes, BDEs at 0 K are determined for the $Cu^+(MeOH)_x$ complexes, where $x = 1-6$. Insight into the structures and BDEs of the $Cu^+(MeOH)_x$ complexes is provided by density functional theory calculations of these complexes performed at the B3LYP/6-311+G(2d,2p)// B3LYP/6-31G* level of theory. NBO analyses also provide insight into the nature of the binding and the preference for hydrogen bonding over further direct solvation of the Cu^+ ion in the larger $Cu^+(MeOH)_x$ complexes, that is, $x \geq 3$. Comparison of the measured and calculated BDEs for the $Cu^+(MeOH)_x$ complexes suggests that only the ground-state conformations of the $Cu^+(MeOH)_x$ complexes, where $x = 1-5$, are accessed in our experiments, whereas three low-energy conformers of $Cu^+(MeOH)_6$ are likely present under our experimental conditions. The ground-state structures of the $Cu^+(MeOH)_x$ complexes and the trends in the sequential BDEs are explained in terms of sd hybridization, electron donor−acceptor natural bond orbital stabilizing interactions, ligand−ligand repulsion, and hydrogen bonding.

Acknowledgment. This work is supported by the National Science Foundation, Grant CHE-0518262.

Supporting Information Available: Table of vibrational frequencies, average vibrational energies at 298 K, and rotational constants of neutral MeOH and the $Cu^+(MeOH)_x$ complexes in their ground-state conformations. Figures showing the B3LYP/6−31G*-optimized geometries and B3LYP/6−311+G(2d,2p) relative stabilities of the stable conformations computed for the $Cu^+(MeOH)_x$ complexes. This material is available free of charge via the Internet at http://pubs.acs.org.

References and Notes

(1) Gelpi, E. *J. Chromatogr., A* **1995**, *703*, 59.
(2) Niessen, W. M. A.; Tinke, A. P. *J. Chromatogr., A* **1995**, *703*, 37.
(3) Slobodnik, J.; van Barr, B. L. M.; Brinkman, U. A. T. *J. Chromatogr., A* **1995**, *703*, 81.
(4) Cech, N. B.; Enke, C. G. *Mass Spectrom. Rev.* **2001**, *20*, 362.
(5) Jackson, G. S.; Enke, C. G. *Anal. Chem.* **1999**, *71*, 3777.
(6) Zhou, S.; Hamburger, M. *Rapid Commun. Mass Spectrom.* **1995**, *9*, 1516.
(7) James, E. H.; Ellen A. K.; Richard, L. K. *Inorganic Chemistry: Principles of Structure and Reactivity*, 4th ed.; Harper Collins College Publications: New York, 1993.
(8) Lippard, S. J.; Berg, J. M.; *Principles of Bioinorganic Chemistry*; University Science Books: Mill Valley, CA, 1994.
(9) Siegbahn, P. E. M. *J. Comput. Chem.* **2001**, *22*, 1634.
(10) Palmer, A. E.; Randall, D. W.; Xu, F.; Solomon, E. I. *J. Am. Chem. Soc.* **1999**, *121*, 7138.
(11) Wang, X.; Berry, S. M.; Xia, Y.; Lu, Y. *J. Am. Chem. Soc.* **1999**, *121*, 7449.
(12) Siegbahn, P. E. M.; Wirstam, M. *J. Am. Chem. Soc.* **2001**, *123*, 11819.
(13) Chowdhury, A.; Peteanu, L. A.; Holland, P. L.; Tolman, W. B. *J. Phys. Chem. B* **2002**, *106*, 3007.
(14) Battistuzzi, G.; Bellei, M.; Borsari, M.; Canters, G. W.; de Waal, E.; Jeuken, L. J. C.; Ranieri, A.; Sola, M. *Biochemistry* **2003**, *42*, 9214.
(15) Donaire, A.; Jimenez, B.; Moratal, J.-M.; Hall, J. F.; Hasnain, S. S. *Biochemistry* **2001**, *40*, 837.
(16) Solomon, E. I.; Szilagyi, R. K.; DeBeer, G. S.; Basumallick, L. *Chem. Rev.* **2004**, *104*, 419.
(17) Burda, J. V.; Šponer, J.; Hobza, P. *J. Phys. Chem.* **1996**, *100*, 7250.
(18) Burda, J. V.; Šponer, J.; Leszczynski, J.; Hobza, P. *J. Phys. Chem. B* **1997**, *101*, 9670.
(19) Gasowska, A.; Lomozik, L. *Monatsh. Chem.* **1995**, *126*, 13.
(20) Šponer, J.; Sabat, M.; Burda, J.; Leszczynski, J.; Hobza, P.; Lippert, B. *J. Biol. Inorg. Chem.* **1999**, *4*, 537.
(21) Sabolovic, J.; Tautermann, C. S.; Loerting, T.; Liedl, K. R. *Inorg. Chem.* **2003**, *42*, 2268.
(22) Sabolovic, J.; Liedl, K. R. *Inorg. Chem.* **1999**, *38*, 2764.
(23) Bertran, J.; Rodrigues-Santiago, L.; Sodupe, M. *J. Phys. Chem. B* **1999**, *103*, 2310.
(24) Rulíšek, L.; Havlas, Z. *J. Am. Chem. Soc.* **2000**, *122*, 10428.
(25) Santra, S.; Zhang, P.; Tan, W. *J. Phys. Chem. A* **2000**, *104*, 12021.
(26) Shoeib, T.; Rodriquez, C. F.; Siu, K. W. M.; Hopkinson, A. C. *Phys. Chem. Chem. Phys.* **2001**, *3*, 853.
(27) Prabhakar, R.; Siegbahn, P. E. M. *J. Phys. Chem. B* **2003**, *107*, 3944.
(28) Manikandan, P.; Epel, B.; Goldfarb, D. *Inorg. Chem.* **2001**, *40*, 781.
(29) Shimizu, K.; Maeshima, H.; Yoshida, H.; Satsuma, A.; Hattori, T. *Phys. Chem. Chem. Phys.* **2001**, *3*, 862.
(30) Tachikawa, H. *Chem. Phys. Lett.* **1996**, *260*, 582.
(31) Schroeder, D.; Schwartz, H.; Wu, J.; Wesdemiotis, C. *Chem. Phys. Lett.* **2001**, *343*, 258.
(32) Marini, G. W.; Liedl, K. R.; Rode, B. M. *J. Phys. Chem. A* **1999**, *103*, 11387.
(33) Schwenk, C. F.; Rode, B. M. *Phys. Chem. Chem. Phys.* **2003**, *5*, 3418.
(34) Feller, D.; Glendening, E. D.; de Jong, W. A. *J. Chem. Phys.* **1999**, *110*, 1475.
(35) Pavelka, M.; Burda, J. V. *Chem. Phys.* **2005**, *312*, 193.
(36) Burda, J. V.; Pavelka, M.; Šimánek, M. *J. Mol. Struct.: THEOCHEM* **2004**, *683*, 183.
(37) Holland, P. M.; Castleman, A. W., Jr. *J. Chem. Phys.* **1982**, *76*, 4195.
(38) Magnera, T. F.; David, D. E.; Stulik, D.; Orth, R. G.; Jonkman, H. T.; Michl, L. *J. Am. Chem. Soc.* **1989**, *111*, 5036.
(39) Dalleska, N. F.; Honma, K.; Sunderlin, L. S.; Armentrout, P. B. *J. Am. Chem. Soc.* **1994**, *116*, 3519.
(40) Stace, A. J.; Walker, N. R.; Wright, R. R.; Firth, S. *Chem. Phys. Lett.* **2000**, *329*, 173.
(41) Stone, J. A.; Vukomanovic, D. *Chem. Phys. Lett.* **2001**, *346*, 419.
(42) Holland, P. M.; Castleman, A. W., Jr. *J. Am. Chem. Soc.* **1980**, *102*, 6175.
(43) Castleman, A. W., Jr.; Weil, K. G.; Sigsworth, S. W.; Leuchter, R. E.; Keesee, R. G. *J. Chem. Phys.* **1987**, *86*, 3829.
(44) Walter, D.; Armentrout, P. B. *J. Am. Chem. Soc.* **1998**, *120*, 3176.
(45) Vitale, G.; Valina, A. B.; Huang, H.; Amunugama, R.; Rodgers, M. T. *J. Phys. Chem. A* **2001**, *105*, 11351.

(46) Chu, Y.; Yang, Z.; Rodgers, M. T. *J. Am. Soc. Mass Spectrom.* **2002**, *13*, 453.
(47) Koizumi, H.; Zhang, X. G.; Armentrout, P. B. *J. Phys. Chem. A* **2001**, *105*, 2444.
(48) Rannulu, N. S.; Rodgers, M. T. *Phys. Chem. Chem. Phys*. **2005**, *7*, 1014.
(49) Rannulu, N. S.; Rodgers, M. T. *J. Phys. Chem. A* **2007**, *111*, 3465.
(50) Valina, A. B.; Amunugama, R.; Huang, H.; Rodgers, M. T. *J. Phys. Chem. A* **2001**, *105*, 11057.
(51) Rodgers, M. T.; Armentrout, P. B. *J. Phys. Chem. A* **1997**, *101*, 1238.
(52) Rodgers, M. T.; Armentrout, P. B. *J. Chem. Phys.* **1998**, *109*, 1787.
(53) Rodgers, M. T.; Ervin, K. M.; Armentrout, P. B. *J. Chem. Phys*. **1997**, *106*, 4499.
(54) Rodgers, M. T. *J. Phys. Chem. A* **2001**, *105*, 2374.
(55) Teloy, E.; Gerlich, D. *Chem. Phys*. **1974**, *4*, 417.
(56) Gerlich, D. *Adv. Chem. Phys*. **1992**, *82*, 1.
(57) Ervin, K. M.; Armentrout, P. B. *J. Chem. Phys*. **1985**, *83*, 166.
(58) Frisch, M. J.; Trucks, G. W.; Schlegel, H. B.; Scuseria, G. E.; Robb, M. A.; Cheeseman, J. R.; Zakrzewski, V. G.; Montgomery, J. A., Jr.; Stratmann, R. E.; Burant, J. C.; Dapprich, S.; Millam, J. M.; Daniels, A. D.; Kudin, K. N.; Strain, M. C.; Farkas, O.; Tomasi, J.; Barone, V.; Cossi, M.; Cammi, R.; Mennucci, B.; Pomelli, C.; Adamo, C.; Clifford, S.; Ochterski, J.; Petersson, G. A.; Ayala, P. Y.; Cui, Q.; Morokuma, K.; Malick, D. K.; Rabuck, A. D.; Raghavachari, K.; Foresman, J. B.; Cioslowski, J.; Ortiz, J. V.; Stefanov, B. B.; Liu, G.; Liashenko, A.; Piskorz, P.; Komaromi, I.; Gomperts, R.; Martin, R. L.; Fox, D. J.; Keith, T.; Al-Laham, M. A.; Peng, C. Y.; Nanayakkara, A.; Gonzalez, C.; Challacombe, M.; Gill, P. M. W.; Johnson, B. G.; Chen, W.; Wong, M. W.; Andres, J. L.; Head-Gordon, M.; Replogle, E. S.; Pople, J. A. *Gaussian 98*, revision A.11; Gaussian, Inc.: Pittsburgh, PA, 2001.
(59) Becke, A. D. *J. Chem. Phys.* **1993**, *98*, 5648.
(60) Lee, C.; Yang, W.; Parr, R. G. *Phys. Rev. B* **1988**, *37*, 785.
(61) Foresman, J. B.; Frisch, Æ. *Exploring Chemistry with Electronic Structure Methods*, 2nd ed.; Gaussian: Pittsburgh, PA, 1996; p 64.
(62) Scott, A. P.; Radom, L. *J. Phys. Chem.* **1996**, *100*, 16502.
(63) Wong, M. W. *Chem. Phys. Lett*. **1996**, *256*, 391.
(64) Boys, S. F.; Bernardi, R. *Mol. Phys*. **1979**, *19*, 553.
(65) van Duijneveldt, F. B.; van Duijneveldt-van de Rijdt; van Lenthe, J. H. C. M. *Chem. Rev.* **1994**, *94*, 1873.
(66) Glendening, E. D.; Badenhoop, J. K.; Reed, A. E.; Carpenter, J. E.; Weinhold, F. *NBO*, version 3.1; Theoretical Chemistry Institute, University of Wisconsin, Madison, WI, 1995.
(67) Muntean, F.; Armentrout, P. B. *J. Chem. Phys.* **2001**, *115*, 1213.
(68) Beyer, T. S.; Swinehart, D. F. *Commun. ACM* **1973**, *58*, 2438.
(69) Pople, J. A.; Schlegel, H. B.; Ragavachari, K.; DeFrees, K.; Binkley, D. J.; Frisch, J. F.; Whitesides, R. F.; Hout, R. F. H. *Int. J. Quantum Chem. Symp.* **1981**, *15*, 269.
(70) Khan, F. A.; Clemmer, D. E.; Schultz, R. H.; Armentrout, P. B. *J. Phys. Chem.* **1993**, *97*, 7978.
(71) Chesnavich, W. J.; Bowers, M. T. *J. Phys. Chem.* **1979**, *83*, 900.
(72) See, for example, Figure 1 in Dalleska, N. F.; Honma, K.; Armentrout, P. B. *J. Am. Chem. Soc.* **1993**, *115*, 12125.
(73) Armentrout, P. B.; Simons, J. *J. Am. Chem. Soc.* **1992**, *114*, 8627.
(74) McKenna, A. G.; McKenna, J. F. *J. Chem. Educ*. **1984**, *61*, 771.